15528

Steady State Operation of Cylindrical Loop Heat Pipe Evaporators

Z. Wang[1], J. M. Ochterbeck[1], J. Perez[2] and P. Rogers[2]
[1] Department of Mechanical Engineering, Clemson University, Clemson, SC 29634 USA
[2] US Army RDECOM-TARDEC, Warren, MI USA

Abstract

The loop heat pipe evaporators operating under steady state conditions were numerically investigated to describe evaporator characteristics and evaluate evaporator performance. Numerical solutions were obtained for conjugate flow and heat transfer in primary evaporator components. Two typical geometrical configurations used for the cylindrical LHP evaporator, non-bayonet evaporator and bayonet evaporator, were considered to examine the bayonet effects on evaporator operation. It was found that the presence of a bayonet significantly affects the flow and heat transfer in the liquid core and helps to prevent vapor bubbles from accumulating inside the liquid core. The influences of input heat flux, inlet liquid subcooling, external loop resistance and effective thermal conductivity of the wick structure on evaporator performance were also studied. It was observed that increasing the applied heat flux and inlet liquid subcooling decreases the maximum temperature in the liquid core and helps to prevent vapor formation in the liquid core, which is favorable for proper evaporator operation. Decreasing the external loop resistance and effective thermal conductivity also decreases the maximum temperature in the liquid core. Additionally, increasing the applied heat flux and liquid subcooling significantly enhances the cooling capability of the liquid in the bayonet. This helps to prevent vapor bubbles from accumulating in the liquid core.

1. Introduction

Loop heat pipes (LHPs) are capillary-driven two-phase heat transfer devices capable of transporting large heat loads over long distances with very small temperature differences across the systems. As a robust, self-starting, and passive two-phase thermal transport device, the LHP technology is rapidly gaining acceptance in both ground and space applications [1-2]. As shown in Figure 1, the primary LHP components include an evaporator, a compensation chamber, vapor and liquid transport lines, and a condenser. The evaporator is the central part of a LHP which is the heat absorbing component and additionally provides capillary pumping head for the fluid circulation. Complicated flow and heat transfer phenomena take place during evaporator operation. The entire loop performance is highly dependent on the flow and heat transfer characteristics in the evaporator, which mainly include [3]: 1) phase conditions in the wick structure, 2) thermal-fluid behavior in the liquid core, and 3) heat link between the evaporator and the compensation chamber. Physical description of these fundamental flow and heat transfer problems is the key to explore the loop operational characteristics. The flow and heat transfer in the evaporator are influenced by many factors, such as [4]: 1) applied heat load, 2) level of inlet liquid subcooling to the evaporator, 3) porous wick characteristics, 4) thermophysical properties of the wick and the working fluid, and 5) evaporator geometry. It is also important to predict the effects of variations in these parameters on evaporator operation for evaluating evaporator performance. Hence, the development of a model on

Report Documentation Page

Form Approved
OMB No. 0704-0188

1. REPORT DATE	2. REPORT TYPE	3. DATES COVERED
13 AUG 2006	**Journal Article**	**13-08-2006 to 13-08-2006**

4. TITLE AND SUBTITLE
STEADY STATE OF CYLINDRICAL LOOP HEAT PIPE EVAPORATORS

5a. CONTRACT NUMBER
5b. GRANT NUMBER
5c. PROGRAM ELEMENT NUMBER

6. AUTHOR(S)
Paul Rogers; J Perez; Z. Wang; J. Ochterbeck

5d. PROJECT NUMBER
5e. TASK NUMBER
5f. WORK UNIT NUMBER

7. PERFORMING ORGANIZATION NAME(S) AND ADDRESS(ES)
Clemson University,Department of Mechanical Engineering ,Clemson,SC,29634

8. PERFORMING ORGANIZATION REPORT NUMBER
; #15528

9. SPONSORING/MONITORING AGENCY NAME(S) AND ADDRESS(ES)
U.S. Army TARDEC, 6501 E.11 Mile Rd, Warren, MI, 48397-5000

10. SPONSOR/MONITOR'S ACRONYM(S)
TARDEC

11. SPONSOR/MONITOR'S REPORT NUMBER(S)
#15528

12. DISTRIBUTION/AVAILABILITY STATEMENT
Approved for public release; distribution unlimited

13. SUPPLEMENTARY NOTES
INTERNATIONAL HEAT TRANSFER CONFERENCE (IHTC-13)

14. ABSTRACT

The loop heat pipe evaporators operating under steady state conditions were numerically investigated to describe evaporator characteristics and evaluate evaporator performance. Numerical solutions were obtained for conjugate flow and heat transfer in primary evaporator components. Two typical geometrical configurations used for the cylindrical LHP evaporator, non-bayonet evaporator and bayonet evaporator, were considered to examine the bayonet effects on evaporator operation. It was found that the presence of a bayonet significantly affects the flow and heat transfer in the liquid core and helps to prevent vapor bubbles from accumulating inside the liquid core. The influences of input heat flux, inlet liquid sub cooling , external loop resistance and effective thermal conductivity of the wick structure on evaporator performance were also studied. It was observed that increasing the applied heat flux and inlet liquid subcooling decreases the maximum temperature in the liquid core and helps to prevent vapor formation in the liquid core, which is favorable for proper evaporator operation. Decreasing the external loop resistance and effective thermal conductivity also decreases the maximum temperature in the liquid core. Additionally increasing the applied heat flux and liquid subcooling significantly enhances the cooling capability of the liquid in the bayonet. This helps to prevent vapor bubbles from accumulating in the liquid core.

15. SUBJECT TERMS

16. SECURITY CLASSIFICATION OF:			17. LIMITATION OF ABSTRACT	18. NUMBER OF PAGES	19a. NAME OF RESPONSIBLE PERSON
a. REPORT **unclassified**	b. ABSTRACT **unclassified**	c. THIS PAGE **unclassified**	**Same as Report (SAR)**	**22**	

Standard Form 298 (Rev. 8-98)
Prescribed by ANSI Std Z39-18

evaporator operation is needed to physically describe evaporator characteristics and allow investigation of individual parameters affecting evaporator performance.

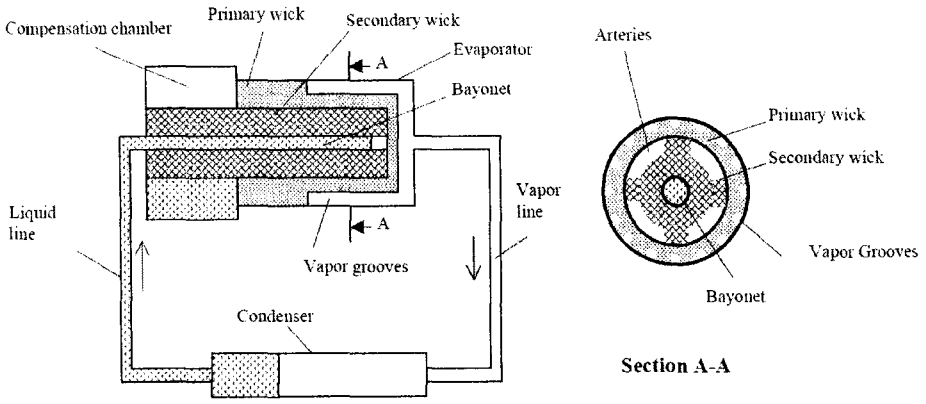

Figure 1- Schematic of the LHP

Kiper et al. [5] firstly applied a lumped heat capacity model for the evaporator to investigate transient evaporator operation. The transient evaporator temperature profile was obtained by solving an overall energy balance of the evaporator. In order to describe the complex physical processes during LHP operation, a simplified thermal network model was presented by Bienert and Wolf [6] where the energy balances were solved using a combined lumped parameter-nodal approach. Using lumped analysis for each component in the loop, the overall loop is simplified to a thermal network while all components become the nodes of the network. The thermodynamic state of the fluid at each location is clearly defined and the energy balance is applied for each element. Based on this thermal network, Kaya and Hoang [7] presented a mathematical model on LHP operation. An analytical, implicit expression of the LHP operating temperature was obtained in their work.

It should be noted that the fluid flow problem is of significant importance in the evaporator and no meaningful conclusions can be made without a combined flow and heat transfer analysis. Wulz and Embacher [8] modeled a flat-plate type evaporator using a steady-state two-dimensional model. The location of the liquid-vapor interface and the interface temperature were prescribed, which are generally unknown, and liquid flow and heat transfer in the wick structure were considered. Cao and Faghri [9-10] presented a mathematical formulation for a flat-plate type evaporator under small or moderate heat fluxes, which includes liquid flow and heat transfer in the porous wick, three-dimensional vapor flow in the groove, and heat transfer in the cover plate. The liquid and vapor flow are coupled via interfacial mass flux, and the entire evaporator is solved as a conjugate problem. For high heat fluxes, Zhao and Liao [11] reported that a two-phase coexistence zone resided into the wick structure. Thus, the two-phase behavior in the porous wick should be considered to model the evaporator at high heat fluxes. Khrustalev and Faghri [12] theoretically investigated the heat transfer in the evaporator at high heat fluxes. It was believed that the stable vapor blanket exists inside the wick structure along the heated surface at extremely high heat fluxes. A one-dimensional model was developed to describe the capillary-driven vapor flow and heat transfer in the dry region of the wick structure. The model predicted the location and shape of the liquid-vapor interface and the working limits of the evaporator. Udell [13] indicated that a heat pipe effect existed in the two-phase zone of porous media, where transport phenomena and fluid flow were similar to conventional heat pipe operation.

Based on this understanding, the transport process in the two-phase zone was hydrodynamically described as a countercurrent two-phase flow [14]. Following the study of Udell [14], Zhao and Liao [11] performed a hydrodynamic analysis on the heat and mass transfer in the two-phase zone of the porous structure. Appling a separated flow approach for the capillary-driven, countercurrent two-phase flow in the two-phase zone, the phase distribution in the porous structure was obtained. Yan and Ochterbeck [4] numerically investigated a cylindrical evaporator operating under steady-state conditions, where the two-phase flow and heat transfer in the wick structure was described by using a two-phase mixture model. It was found that either increasing the applied heat flux and/or the liquid sub-cooling resulted in decreased liquid core temperature, which helps prevent bubble formation in the evaporator core, and is therefore favorable for proper evaporator operation.

Most existing models are phenomenological or semi-empirical, which lack sufficient prior knowledge of the fundamental flow and heat transfer characteristics and therefore can not explain the physical mechanisms of many basic phenomena in the evaporator [15]. In order to develop a model for comprehensively describing evaporator behavior and accurately predicting the effects of variations in operational parameters on evaporator operation, fundamentals related to flow and heat transfer in the evaporator must be intensively studied. To date, only a few studies have been reported in this field, and fewer have included these fundamentals in their modeling efforts [1, 4]. In the present study, the steady state operation of cylindrical LHP evaporators was numerically investigated to describe evaporator characteristics and evaluate evaporator performance. Two typical geometrical configurations used for the cylindrical LHP evaporator, non-bayonet evaporator and bayonet evaporator, were considered to examine the bayonet effects on evaporator operation. Operational parameters affecting flow and heat transfer in the evaporator were also studied to evaluate evaporator performance.

2. Physical Model of the LHP Evaporators

Two types of cylindrical LHP evaporators employed in this study were schematically shown in Figure 2, where the primary difference between these two evaporators is the geometric configuration used for the liquid core in the evaporator. As shown in Figure 2, there are typically two geometric configurations used for the evaporator core in practical applications:

1) Circular core of the non-bayonet evaporator (Figure 2(a)): the extension of the liquid return line serves as the evaporator core.
2) Annular core of the bayonet evaporator (Figure 2(b)): a bayonet is inserted into the liquid core.

In the present study, both configurations were considered to examine the effects of bayonet on the evaporator operation.

The physical model of cylindrical LHP evaporators is shown in Figure 3. For the non-bayonet evaporator, liquid returning from the condenser enters the evaporator through the liquid core. In the circular core, the liquid is drawn into the porous wick due to capillary forces. Finally, the vaporization of liquid take places at the outer surface of the wick structure. Hence in the non-bayonet evaporator, two distinct computational domains can be defined for the liquid core and the wick structure (see Figure 3(a)). For simplicity, a full-length bayonet was employed in the bayonet evaporator, where the bayonet length is nearly equal to the evaporator length.

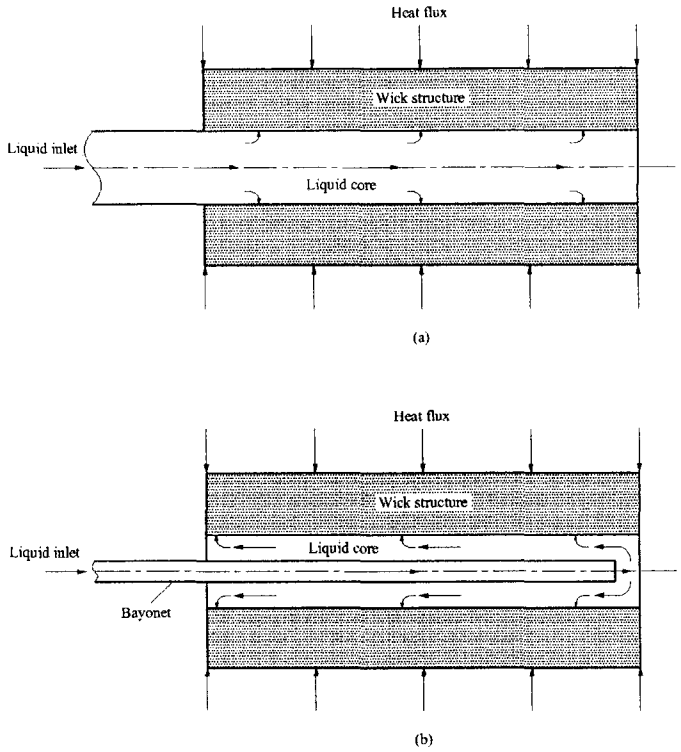

Figure 2- Flow schematic of the cylindrical LHP evaporator: (a) non-bayonet evaporator and (b) bayonet evaporator.

For such circumstance, three computational domains can thus be designated for the bayonet, the liquid core and the wick structure in the bayonet evaporator, respectively (see Figure 3(b)). The flow and heat transfer in these domains are coupled due to heat and mass connections at domain boundaries. In this study, the steady state evaporator operation was numerically simulated as conjugate flow and heat transfer in primary evaporator components. As a conjugate problem, governing equations were applied for each domain respectively which should be solved simultaneously with conjugate boundary conditions at domain boundaries. As the evaporator is taken to be symmetric, the two-dimensional cylindrical coordinates were applied in the physical model, as shown in Figure 3. Other important assumptions in the evaporator model are introduced as:

1) For the flow and heat transfer in the evaporator, the thermophysical properties of the liquid were approximated to be constant and correspond to the saturation temperature in the compensation chamber, T_{cc}. This assumption was based on the fact that the temperature variation in the evaporator is usually small.
2) Gravitational effects are neglected.
3) The vapor flow in the vapor channel was neglected.
4) The heat conduction in the cover plate and metal bayonet wall were negligible.

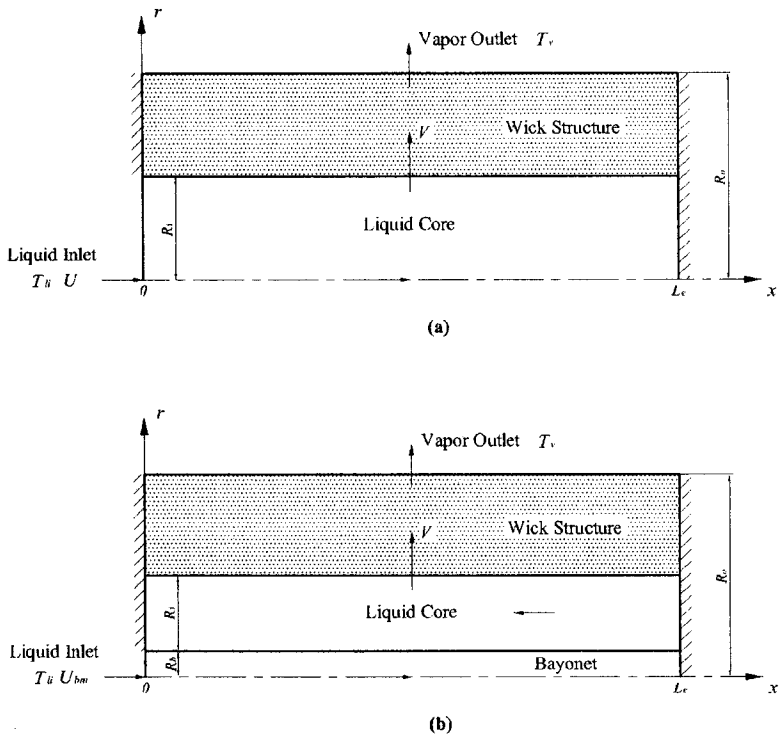

Figure 3- Physical model of cylindrical LHP evaporators: (a) non-bayonet evaporator and (b) bayonet evaporator.

3. Flow and Heat Transfer in the Liquid Core

3.1. Circular Core

The following major assumptions were made for the flow and heat transfer in the circular core, as shown in Figure 3(a):

1) The liquid flow in the liquid core is incompressible and laminar.
2) Since the flow in the liquid return line is fully developed and adiabatic, it was assumed that the flow at the inlet of the liquid core is fully developed and the inlet temperature is uniform.
3) The outlet velocity at the wick/core interface is uniform due to the presence of the porous structure.

Governing Equations

Continuity

$$\frac{\partial u}{\partial x}+\frac{1}{r}\frac{\partial}{\partial r}(rv)=0 \tag{1}$$

Momentum

$$\frac{\partial(u^2)}{\partial x}+\frac{1}{r}\frac{\partial(ruv)}{\partial r}=-\frac{1}{\rho_l}\frac{\partial P}{\partial x}+\nu_l\left[\frac{\partial^2 u}{\partial x^2}+\frac{1}{r}\frac{\partial}{\partial r}\left(r\frac{\partial u}{\partial r}\right)\right] \quad (2)$$

$$\frac{\partial(uv)}{\partial x}+\frac{1}{r}\frac{\partial(rv^2)}{\partial r}=-\frac{1}{\rho_l}\frac{\partial P}{\partial r}+\nu_l\left[\frac{\partial^2 v}{\partial x^2}-\frac{v}{r^2}+\frac{1}{r}\frac{\partial}{\partial r}\left(r\frac{\partial v}{\partial r}\right)\right] \quad (3)$$

Energy

$$\frac{\partial(uT)}{\partial x}+\frac{1}{r}\frac{\partial(rvT)}{\partial r}=\alpha_l\left[\frac{\partial^2 T}{\partial x^2}+\frac{1}{r}\frac{\partial}{\partial r}\left(r\frac{\partial T}{\partial r}\right)\right] \quad (4)$$

Boundary Conditions

The boundary conditions can be described by the following equations:

At $x=0$:

$$u(r)=2U\left[1-\left(\frac{r}{R_i}\right)^2\right] \quad (5) \qquad v=0 \quad (6) \qquad T=T_{li} \quad (7)$$

At $x=L_e$:

$$u=0 \quad (8) \qquad v=0 \quad (9) \qquad \frac{\partial T}{\partial x}=0 \quad (10)$$

At $r=0$:

$$\frac{\partial u}{\partial r}=0 \quad (11) \qquad v=0 \quad (12) \qquad \frac{\partial T}{\partial r}=0 \quad (13)$$

At $r=R_i$:

$$u=0 \quad (14) \qquad v=\frac{R_i}{2L_e}U \quad (15)$$

Equations (5) to (7) are the boundary conditions at the inlet of the liquid core, where the flow was assumed to be fully developed laminar with a uniform inlet temperature, T_{li}. In Equation (5), the mean velocity, U, in the liquid core can be obtained by performing an overall heat balance on the evaporator as

$$U=\frac{1}{\rho_l R_i^2}\frac{2R_o L_e q''_w}{h_{fg}+c_p(T_v-T_{li})} \quad (16)$$

In the above equation, it is assumed that the sensible heat absorbed by the vapor is negligible and the liquid temperature at the outer surface of the wick is nearly equal to the vapor temperature in the vapor grooves, T_v. Basically, there are two saturation states for the LHP operation: one situates at the evaporating interface in the evaporator grooves while another saturation state which represents the compensation chamber exists in the liquid return line [3]. Because these two saturation states are thermodynamically related, the following condition must be satisfied for the loop system [16]:

$$\Delta P_{tot} - \Delta P_w = \left(\frac{\partial P}{\partial T}\right)_{sat} \left(T_v - T_{cc}\right), \tag{17}$$

where the slope of the vapor-pressure curve, $(\partial P/\partial T)_{sat}$, can be related to thermophysics properties by using the Clapeyron equation:

$$\left(\frac{\partial P}{\partial T}\right)_{sat} = \frac{h_{fg}}{T_{sat}\Delta v_{fg}}. \tag{18}$$

Thus, T_v can be written as

$$T_v = T_{cc}\left(1 + \frac{\Delta v_{fg}}{h_{fg}}\Delta P_{ext}\right), \tag{19}$$

where the external loop resistance $\Delta P_{ext} = \Delta P_{tot} - \Delta P_w$. Equations (8) to (10) state that the far end of the liquid core is impermeable and adiabatic. Equations (11) to (13) indicate that the velocity and temperature fields are symmetric about the centerline of the circular core. Equations (14) and (15) specify that the outlet velocity at the wick/core interface is uniform due to the existence of the porous structure.

3.2. Annular Core

In practical applications, a bayonet core design is often utilized for the LHP evaporator, where a bayonet is inserted into the liquid core. As shown in Figure 2(b), liquid returning from the condenser flows inside the bayonet and then flows backward in the annular core between the bayonet and the wick. Compared with the circular core, this reverses the main flow direction in the liquid core and thus moves the stagnation point from the vapor end to the liquid end where the liquid in the bayonet has maximum subcooling. As a consequence, this configuration forces any vapor present in the liquid core to flow to the inlet section of the evaporator where it can be collapsed by exchanging heat with the incoming subcooled liquid or easily vents to the compensation chamber.

For simplicity, a full-length bayonet was employed in the present study where the bayonet length is nearly equal to the evaporator length. Liquid exiting from the bayonet immediately enters the annular core with a uniform velocity and temperature. In the annular core, the liquid is heated by the wick surface while it is cooled by the subcooled liquid in the

bayonet. During liquid flow in the liquid core, liquid is drawn into the porous wick due to capillary forces. As shown in Figure 3(b), the same governing equations (1) to (4) can be still applied for the flow and heat transfer in the annular core with new boundary conditions:

At $x = 0$:

$u = 0$ (20) $\quad v = 0$ (21) $\quad \dfrac{\partial T}{\partial x} = 0$ (22)

At $x = L_e$:

$u = U_{ci}$ (23) $\quad v = 0$ (24)

At $r = R_b$:

$u = 0$ (25) $\quad v = 0$ (26)

At $r = R_i$:

$u = 0$ (27) $\quad v = V = -\dfrac{R_i^2 - R_b^2}{2R_i L_e} U_{ci}$ (28)

Due to the presence of the bayonet, the stagnation end of the annular core situates at the liquid inlet end of the evaporator. Equations (20) to (22) state that the stagnation end is impermeable and adiabatic. Equations (23) and (24) are the boundary conditions at the inlet of the annular core, where the inlet liquid velocity ~~were~~ was assumed to be uniform. In Eq. (23), the inlet velocity, U_{ci}, in the liquid core is given by

$$U_{ci} = -\frac{2R_o L_e q_w'' / \rho_l \left(R_i^2 - R_b^2\right)}{h_{fg} + c_p \left(T_v - T_{li}\right)} \tag{29}$$

Equations (25) and (26) are no-slip velocity boundary conditions on the outer surface of the bayonet. Equations (27) and (28) specify that the outlet velocity at the wick/core interface is uniform due to the existence of the porous structure.

4. Flow and Heat Transfer in the Bayonet

For fully developed laminar flow in the bayonet, the following parabolic velocity profile can be obtained:

$$u(r) = 2U_{bm}\left[1 - \left(\frac{r}{R_i}\right)^2\right] \tag{30}$$

where the mean velocity, U_{bm}, in the bayonet can be written as

$$U_{bm} = \frac{1}{\rho_l R_b^2} \frac{2R_o L_e q''_w}{h_{fg} + c_p (T_v - T_{li})} \tag{31}$$

The energy equation for the flow and heat transfer in the bayonet is expressed as

$$u \frac{\partial T}{\partial x} = \alpha_l \left[\frac{\partial^2 T}{\partial x^2} + \frac{1}{r} \frac{\partial}{\partial r} \left(r \frac{\partial T}{\partial r} \right) \right] \tag{32}$$

The boundary conditions for the bayonet are given by:

At $x = 0$:

$$T = T_{li} \tag{33}$$

At $r = 0$:

$$\frac{\partial T}{\partial r} = 0 \tag{34}$$

Equation (33) specifies the inlet liquid temperature of the evaporator, T_{li}, as the boundary condition at the inlet of the bayonet ($x = 0$) while no boundary condition is needed to be specified at the outflow boundary ($x = L_e$) for the fully developed pipe flow in the bayonet. Equation (34) indicates that the temperature field is symmetric about the centerline of the bayonet.

5. Flow and Heat Transfer in the Wick Structure

For the flow and heat transfer in the wick structure, the following major assumptions were made:

1) The porous wick is rigid, homogeneous, and isotropic.
2) The wick is fully saturated with liquid before the presence of a two-phase zone in the wick structure, where vaporization of the liquid takes place exclusively from the outer surface of the wick.
3) Darcy's law is applicable to the liquid flow in the wick structure.
4) The liquid and solid phases are in local thermal equilibrium.
5) It was assumed that the temperature at the outer surface of the wick is nearly equal to the vapor temperature in the vapor grooves.

3 Adjust font size

Governing Equations

Continuity

$$\frac{\partial u}{\partial x} + \frac{1}{r} \frac{\partial}{\partial r} (rv) = 0 \tag{35}$$

Momentum

$$u = -\frac{K}{\mu}\frac{\partial P}{\partial x} \tag{36}$$

$$v = -\frac{K}{\mu}\frac{\partial P}{\partial r} \tag{37}$$

Energy

$$u\frac{\partial T}{\partial x} + v\frac{\partial T}{\partial r} = \alpha_{eff}\left[\frac{\partial^2 T}{\partial x^2} + \frac{1}{r}\frac{\partial}{\partial r}\left(r\frac{\partial T}{\partial r}\right)\right] \tag{38}$$

Boundary Conditions

The boundary conditions can be described by the following equations:

At $x = 0$:

$u = 0$ (39) $\qquad \frac{\partial T}{\partial x} = 0$ (40)

At $x = L_e$:

$u = 0$ (41) $\qquad \frac{\partial T}{\partial x} = 0$ (42)

At $r = R_i$:

$u = 0$ (43) $\qquad v = V$ (44)

At $r = R_o$:

$u = 0$ (45) $\qquad T = T_v$ (46)

Equations (39) to (42) indicate that the left and right boundaries of the wick structure are impermeable and adiabatic because no heat or mass exchange occurs at the boundaries. Equations (43) and (44) come from Eqs. (27) and (28) which represent the mass connection at the wick/core interface. Equation (46) states that the temperature at the outer surface of the wick is assumed to be the vapor temperature in the vapor grooves.

The above boundary conditions suggest that the axial velocity component in the wick structure is zero. Thus, the velocity profile in the wick structure can be directly determined by the continuity equation (35) as

$$u = 0 \tag{47}$$

$$v = \frac{R_i}{r} V \tag{48}$$

Therefore, the energy equation (38) becomes

$$v\frac{\partial T}{\partial r} = \alpha_{eff}\left[\frac{\partial^2 T}{\partial x^2} + \frac{1}{r}\frac{\partial}{\partial r}\left(r\frac{\partial T}{\partial r}\right)\right] \tag{49}$$

6. Heat and Mass Connections between Components

The flow and heat transfer in the LHP evaporator is characterized by the heat and mass connection between each component. Therefore, the steady state evaporator operation was solved as a conjugate problem of flow and heat transfer in the bayonet, the liquid core and the wick structure, where the flow and heat transfer in each domain can be coupled by conjugate boundary conditions at domain boundaries. Conjugate boundary conditions exist at the core/bayonet interface ($r = R_b$) and the wick/core interface ($r = R_i$), where temperatures and heat fluxes at the boundaries on both sides should be equal. These boundary conditions can be expressed as:

At $r = R_b$:

$$T\big|_{r=R_b^-} = T\big|_{r=R_b^+} \tag{50}$$

$$\left.\frac{\partial T}{\partial r}\right|_{r=R_b^-} = \left.\frac{\partial T}{\partial r}\right|_{r=R_b^+} \tag{51}$$

At $r = R_i$:

$$T\big|_{r=R_i^-} = T\big|_{r=R_i^+} \tag{52}$$

$$\lambda_l \left.\frac{\partial T}{\partial r}\right|_{r=R_i^-} = \lambda_{eff} \left.\frac{\partial T}{\partial r}\right|_{r=R_i^+} \tag{53}$$

Equations (50) and (51) are based on the assumption that the heat transfer in the bayonet wall is negligible. It should be noted that there also is a heat and mass connection between the outlet of the bayonet and the inlet of the annular core. In this model, it was assumed that liquid exiting from the bayonet immediately enters the annular core with a uniform velocity and temperature. Hence, the temperature at the inlet of the liquid core was assumed to be equal to the temperature at the outlet of the bayonet.

7. Numerical Treatment

A finite difference method is used to solve the governing equations for the flow and heat transfer in the bayonet, the liquid core and the wick structure. A uniform staggered grid

mesh was used in the present study. In this grid scheme, the main grid points are located at the center of the control volume. The finite difference equations were formulated using the control volume approach, where the power law scheme [17] was applied to represent the transport properties on the control volume surfaces. A SIMPLER algorithm proposed by Patankar [17] was utilized to calculate the flow field. As the boundary conditions at both the wick/core and core/bayonet interfaces were unknown, the temperature fields were solved as a conjugate problem. The procedures for solving this conjugate problem can be introduced as:

1) Assume a heat flux distribution at the core/bayonet interface.
2) Calculate the temperature field in the bayonet with the guessed heat flux boundary condition.
3) Obtain the temperature at the core/bayonet interface and treat this temperature as the boundary condition for the energy equation in the liquid core.
4) Obtain the temperature at the outlet of the bayonet and treat this temperature as the inlet boundary condition for the liquid core.
5) Assume a heat flux distribution at the wick/core interface.
6) Calculate the temperature field in the liquid core with the conjugate boundary conditions obtained from steps (3) to (5).
7) Obtain the temperature at the wick/core interface and treat this temperature as the inlet boundary condition for the wick structure.
8) Calculate the temperature field in the wick structure with the boundary condition obtained from step (7).
9) Calculate the heat flux at the wick/core interface and use this heat flux as the updated boundary condition at the outlet of the liquid core.
10) Repeat steps (6) to (9) till convergence achieved at the wick/core interface.
11) Calculate the heat flux at the core/bayonet interface and use this heat flux as the updated boundary condition for the bayonet.
12) Return to step (2) and repeat until convergence

The convergence criterion of the numerical solution for the velocity and temperature fields was that the relative errors between two consecutive iterations are less than 10^{-8}. The total mass and energy balances were also ensured to be within 0.1% error after convergence was achieved.

8. Results and Discussions

Numerical calculations were carried out for cylindrical LHP evaporators (including non-bayonet and bayonet designs) with the following parameters:

a) Working fluid: ammonia ($T_{cc} = 300K$)
b) Wick inner radius: $R_i = 6mm$
c) Wick outer radius: $R_o = 12mm$
d) Bayonet outer radius for the bayonet evaporator: $R_b = 1.5mm$
e) Evaporator length: $L_e = 50mm$
f) Input heat flux: $q''_w = 20kW/m^2, 30\,kW/m^2$ and $50\,kW/m^2$
g) Inlet liquid subcooling: $\Delta T_{sub,li} = T_{cc} - T_{li} = 5K$ and $10K$

h) Wick effective thermal conductivity: $\lambda_{eff} = 10W/m \cdot K$ and $1\,W/m \cdot K$

i) External loop resistance: $\Delta P_{ext} = 40kPa$ (or $T_v = 301.25\,K$) and $\Delta P_{ext} = 10kPa$ (or $T_v = 300.3125K$)

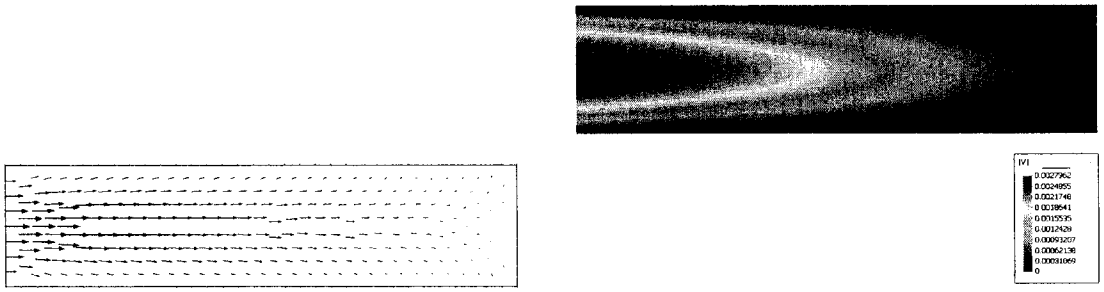

(a) (b)

Figure 4- Velocity field for flow in the circular core ($q''_w = 30kW/m^2$, $\Delta T_{sub,li} = 5K$, $\lambda_{eff} = 10W/m \cdot K$, $\Delta P_{ext} = 40kPa$): (a) velocity vector field and (b) contour of velocity norm, $|V|$

For the non-bayonet evaporator, the grid scheme used were 100×60 and 100×61 for the liquid core and the wick structure, respectively. In the case of the bayonet evaporator, the grid scheme used were 100×50, 100×45 and 100×61 for the bayonet, the liquid core and the wick structure, respectively.

A representative solution of the flow and heat transfer in the non-bayonet evaporator is shown in Figures 4 and 5. For this case, the applied heat flux, inlet liquid subcooling, effective thermal conductivity and external loop resistance are $30kW/m^2$, 5K, $10W/m \cdot K$ and $40kPa$, respectively. The flow field in the circular liquid core is shown in Figure 4. Figure 4(a) shows that the liquid enters the liquid core with a fully developed velocity profile and exists into the wick with a uniform velocity at the wick/core interface.

Since the liquid is drawn into the wick structure due to capillary forces, the mass flow rate or level of velocity norm, $|V|$, drops along the main flow direction and the flow is stagnant at the far end of the liquid core, as shown in Figure 4(b).

Figure 5 illustrates the temperature distribution in the circular core. At the inlet of the liquid core, the temperature is uniform and equal to 295K. In the liquid core, the temperature increases gradually along the main flow direction and also increases monotonically with the radial position. As a result, the maximum temperature appears at the far end of the wick/core interface ($r = 6mm$). It is suggested that the vapor may be generated on the inner wick surface near the far end of the circular liquid core.

A representative solution of the flow and heat transfer in the bayonet evaporator is shown in Figures. 6 to 9. For this case, the heat flux, liquid subcooling, effective thermal conductivity and external loop resistance are $30kW/m^2$, $5K$, $10W/m \cdot K$ and $40kPa$, respectively.

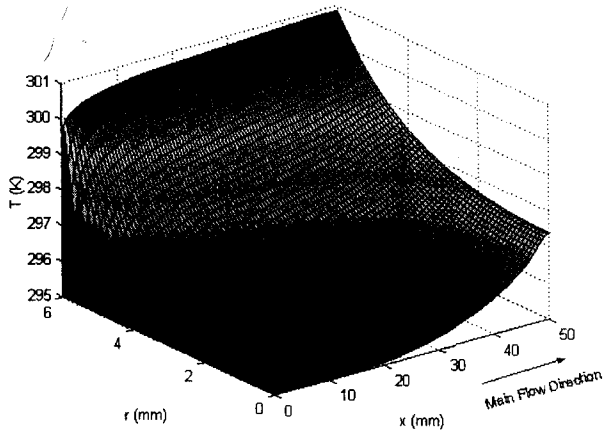

Figure 5 - Temperature distribution in the circular core ($q_w'' = 30kW/m^2$, $\Delta T_{sub.li} = 5K$, $\lambda_{eff} = 10W/m \cdot K$, $\Delta P_{ext} = 40kPa$)

The flow field in the annular core is shown in Figure 6, where the flow direction in the liquid core is reversed and the stagnation point locates at the liquid end of the evaporator due to the presence of a bayonet. Figure 7 illustrates the temperature distribution in the bayonet which is significantly influenced by the heat exchange between the bayonet and the liquid core. In the center region of the bayonet, the temperature gradually increases along the main flow direction due to the heat transfer from the liquid core to the bayonet while the temperature profile close to the bayonet wall is directly affected by the temperature field in the liquid core. It can be concluded that the subcooled liquid in the bayonet serves ~~to be~~ as a heat sink for the liquid core, especially the liquid at the inlet of the bayonet which has the maximum subcooling level. Figure 8 shows the temperature distribution in the liquid core. Liquid exiting from the bayonet immediately enters the annular core with a nearly uniform temperature. In the liquid core, the liquid is heated by the wick surface, where the temperature near the wick surface increases gradually along the flow direction and also increases monotonically with the radial position.

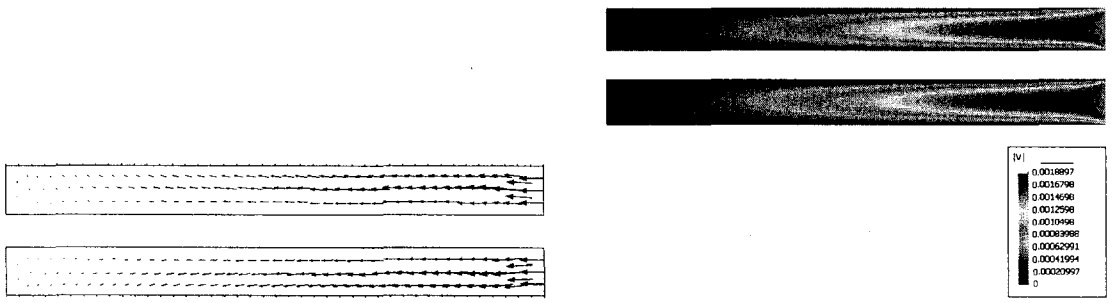

(a) (b)

Figure 6- Velocity field for flow in the annular core ($q_w'' = 30kW/m^2$, $\Delta T_{sub.li} = 5K$, $\lambda_{eff} = 10W/m \cdot K$, $\Delta P_{ext} = 40kPa$): (a) velocity vector field and (b) contour of velocity norm, $|V|$

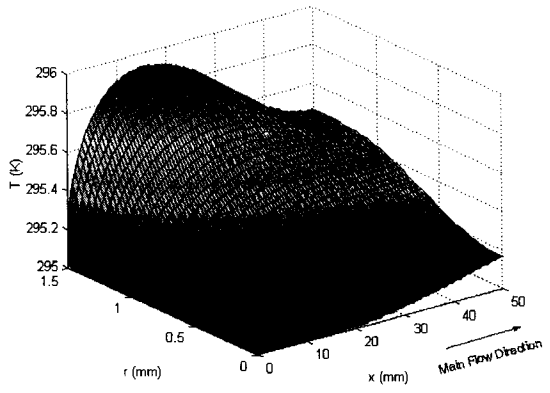

Figure 7- Temperature distribution in the bayonet ($q_w'' = 30kW/m^2$, $\Delta T_{sub.li} = 5K$, $\lambda_{eff} = 10W/m \cdot K$, $\Delta P_{ext} = 40kPa$)

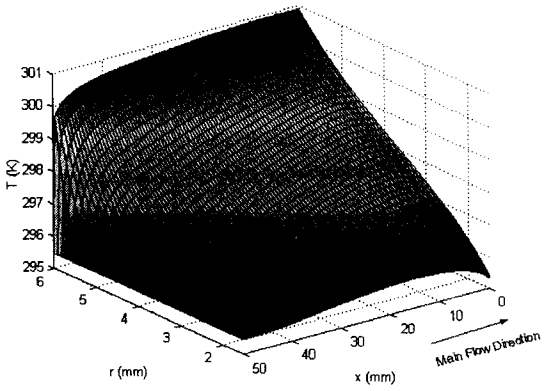

Figure 8- Temperature distribution in the liquid core ($q_w'' = 30kW/m^2$, $\Delta T_{sub.li} = 5K$, $\lambda_{eff} = 10W/m \cdot K$, $\Delta P_{ext} = 40kPa$)

As a result, the maximum temperature appears at the stagnation point of the outlet of the liquid core, where the liquid is superheated. It is suggested that the vapor may be generated on the inner wick surface near the stagnation end of the liquid core. It can be also observed from Figure 8 that the temperature near the bayonet increases initially and drops afterwards along the flow direction. This behavior is due to the fact that there is heat dissipation from the liquid core to the bayonet. Due to this cooling effect, the vapor present at the stagnation end can be collapsed by exchanging heat with the incoming subcooled liquid in the bayonet. Figure 9 shows the temperature distribution in the wick structure. In the wick structure, the temperature gradually increases along the liquid flow direction. At the outlet of the wick structure, the maximum temperature is 301.25K, which is nearly equal to the vapor saturation temperature in the vapor grooves.

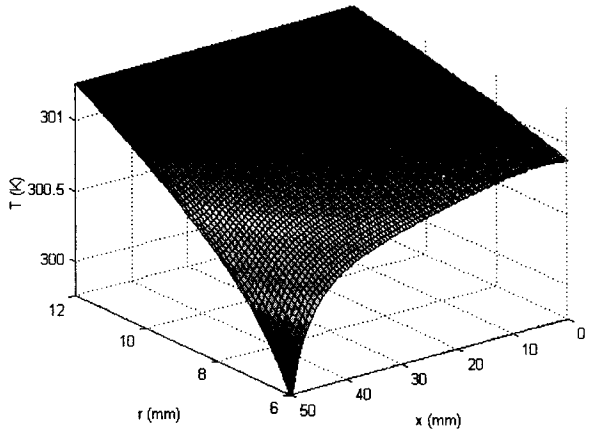

Figure 9- Temperature distribution in the wick structure ($q_w'' = 30kW/m^2$, $\Delta T_{sub.li} = 5K$, $\lambda_{eff} = 10W/m \cdot K$, $\Delta P_{ext} = 40kPa$)

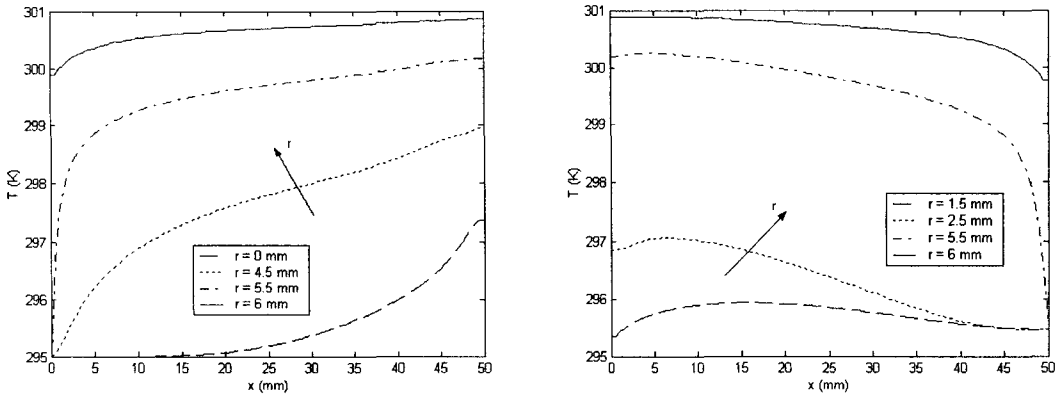

(a) (b)

Figure 10- Variations of temperature profile in the radial position ($q''_w = 30kW/m^2$, $\Delta T_{sub,li} = 5K$, $\lambda_{eff} = 10W/m \cdot K$, $\Delta P_{ext} = 40kPa$): (a) circular core and (b) annular core

8.1. Bayonet effects

Figure 10 shows that the temperature distribution in the annular core is similar to that in the circular core except the temperature reversion in the x-direction. Consequently, the maximum temperature appears at the liquid end ($x = 0$) in the annular core while it appears at the vapor end ($x = L_e$) in the circular core (see Figure 11).

It can be also observed from Figure 10(b) that the temperature near the bayonet increases initially and drops afterwards along the flow direction. This behavior is due to the fact that there is heat dissipation from the liquid core to the bayonet. This results in the vapor presence at the inlet liquid end of the evaporator for the annular core where it can be collapsed by exchanging heat with the incoming subcooled liquid in the bayonet.

Comparisons of the results of flow and heat transfer in the circular core and annular core lead to the following conclusions for bayonet effects on evaporator operation:

1) "Reversal" Effect (x-direction): the presence of a bayonet reverses the main flow direction in the liquid core, and thus reverses the temperature field (see Figure 11).
2) "Cooling" Effect (r-direction): for the circular core, the liquid is heated along the flow direction and the temperature gradually increases (see Figure 10(a)). However in the annular core, the liquid is cooled by the subcooled liquid in the bayonet as well as heated by the wick surface. As a result, along the flow direction in the annular core the liquid temperature increases initially and drops afterwards due to heat dissipation to the liquid in the bayonet (see Figure 10(b)). It can be also observed from Figure 10(b) that this "cooling" effect is obvious only in the region close to the bayonet. For the region far from the bayonet, this effect tends to attenuate, and finally it vanishes in the wick structure.

Due to the above effects, the presence of the bayonet forces any vapor present in the liquid core to flow to the inlet liquid end of the evaporator where it can be collapsed by exchanging heat with the incoming subcooled liquid in the bayonet. The bayonet core design significantly

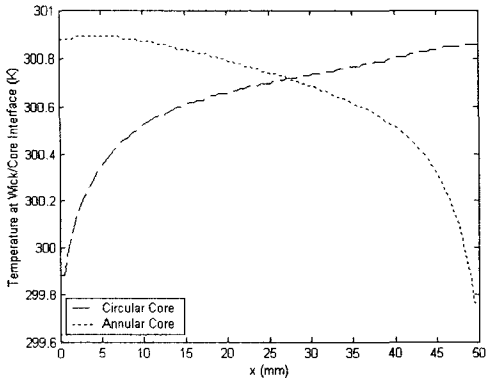

Figure 11- Comparison of temperature distributions at the wick/core interface ($q_w'' = 30kW/m^2$, $\Delta T_{sub.li} = 5K$, $\lambda_{eff} = 10W/m \cdot K$, $\Delta P_{ext} = 40kPa$)

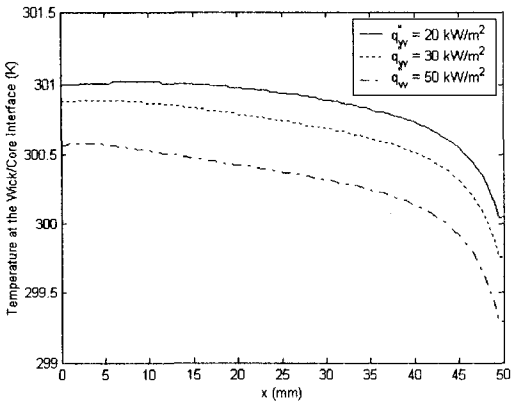

Figure 12 - Influence of heat flux on temperature at the wick/core interface ($\Delta T_{sub.li} = 5K$, $\lambda_{eff} = 10W/m \cdot K$, $\Delta P_{ext} = 40kPa$)

affects the flow and heat transfer in the liquid core and helps to prevent vapor bubbles from accumulating inside the core.

8.2. Heat Flux Effects

The flow and heat transfer in the evaporator is characterized by the heat and mass connection between each component or flow domain. The temperature profiles at the domain boundaries, including the wick/core interface and core/bayonet interface, give a good representation for the flow and heat transfer characteristics in the evaporator, which includes sufficient flow and heat transfer information, such as the heat exchanges between each flow domain, the thermal-fluid behavior in the liquid core and the cooling capability of the liquid in the bayonet.

adjust spacing

Figure 12 shows the effect of heat flux on the temperature at the wick/core interface, where the temperature decreases with the input heat flux. The heat flux applied on the outer surface of the wick structure is transferred in two ways: 1) to the liquid core by conduction and 2) to the vapor channel by convection. The temperature at the wick/core interface is highly related to the heat leak from the wick to the liquid core. Increasing the heat flux increases the system mass flow rate and thus increases the heat convection. As a result, the heat conduction to the liquid core decreases. It is also seen from Figure 12 that the temperature at the stagnation point ($x = 0$) is greater than the saturation temperature ($T_{cc} = 300K$), which indicates vapor formation on the inner surface of the wick. Increasing the heat flux decreases the maximum temperature in the liquid core and helps to prevent vapor formation.

Figure 13 shows the effect of heat flux on the temperature at the core/bayonet interface, where the temperature also decreases with the heat flux. The temperature at the core/bayonet interface is highly involved with the heat dissipation from the liquid core to the bayonet and gives a good representation for the cooling capability of the subcooled liquid in

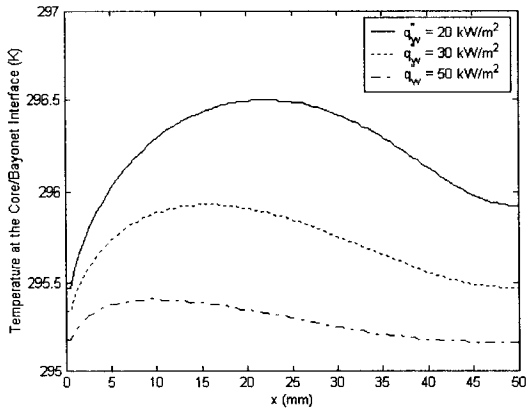

Figure 13 - Influence of heat flux on temperature at the core/bayonet interface ($\Delta T_{sub,li} = 5K$, $\lambda_{eff} = 10W/m \cdot K$, $\Delta P_{ext} = 40kPa$)

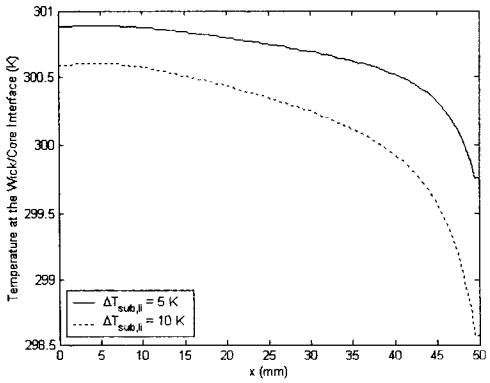

Figure 14- Influence of inlet liquid subcooling on temperature at the wick/core interface ($q''_w = 30kW/m^2$, $\lambda_{eff} = 10W/m \cdot K$, $\Delta P_{ext} = 40kPa$)

the bayonet. Increasing the heat flux increases the mass flow rate in the bayonet and thus increases the cooling capability. Due to this cooling effect, the vapor present in the liquid core can be collapsed by exchanging heat with the incoming subcooled liquid in the bayonet.

8.3. Liquid Subcooling Effects

Figures 14 and 15 present the influence of inlet liquid subcooling on the evaporator operation. Figure 14 shows the liquid subcooling effects on the temperature at the wick/core interface. As expected, the temperature at the wick/core interface decreases with increasing liquid subcooling. Calculations also were conducted for an inlet liquid subcooling level of 20K, where it was observed that the liquid in the liquid core is completely subcooled. Hence, increasing liquid subcooling aids in preventing vapor formation in the liquid core.

Figure 15 shows the effect of inlet liquid subcooling on the temperature at the core/bayonet interface. As seen, the liquid subcooling has a significant influence on the cooling effect of the subcooled liquid in the bayonet. Increasing liquid subcooling greatly decreases the temperature at the core/bayonet interface, which means that the cooling capability of the liquid in the bayonet is significantly enhanced by the increase of the inlet liquid subcooling.

8.4. External Loop Resistance Effects

Figures 16 and 17 show the influence of external loop resistance on the flow and heat transfer in the evaporator. The effect of external resistance on the temperature at the wick/core interface is shown in Figure 16, where the temperature at the wick/core interface increases with the external loop resistance. For a given saturation temperature in the compensation chamber, Equation (19) indicates that the vapor saturation temperature in the vapor channels is determined by the external loop resistance. In this study, it was assumed that the temperature at the outer surface of the wick structure is nearly equal to the vapor temperature in the vapor grooves. Increasing the external loop resistance increases the temperature at the outer surface of wick and thus increases the heat load imposed on the wick surface. As a consequence, the heat transfer from the wick to the liquid core increases. Figure 16 also

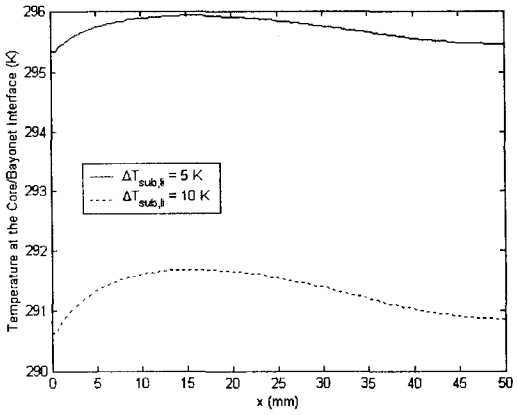

Figure 15- Influence of inlet liquid sub-cooling on temperature at the core/ bayonet interface ($q''_w = 30kW/m^2$, $\lambda_{eff} = 10W/m \cdot K$, $\Delta P_{ext} = 40kPa$)

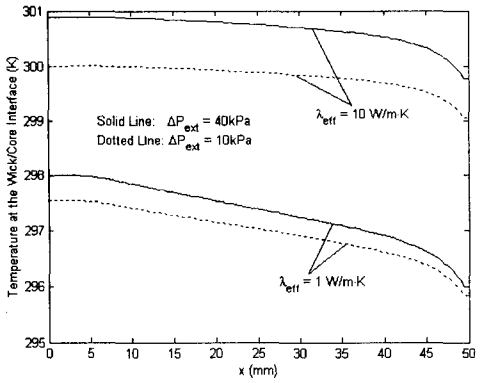

Figure 16- Influence of λ_{eff} and ΔP_{ext} on temperature at the wick/core interface ($q''_w = 30kW/m^2$, $\Delta T_{sub.li} = 5K$)

indicates that the liquid in the liquid core is subcooled for an external resistance of 10kPa. When the external resistance is increased to 40 kPa, it is observed that the liquid at the outlet of the liquid core becomes superheated, which means that vapor may be generated in the liquid core under such condition. Figure 17 shows that the temperature at the core/bayonet interface slightly increases with the external resistance, which suggested that the influence of the external resistance on the cooling capability of the liquid in the bayonet is of insignificance.

8.5. Effective Thermal Conductivity Effects

Figures 16 and 17 also illustrate the influence of the effective thermal conductivity on the temperature at the wick/core interface and the temperature at the core/bayonet interface, respectively. Figure 16 shows the effect of effective thermal conductivity on the temperature at the wick/core interface, where the temperature greatly increases with the effective thermal conductivity. As mentioned above, the input heat load on the outer surface of the wick is transferred partially by conduction to the liquid core and convection to the vapor channel. Increasing effective thermal conductivity increases the heat transfer to the core, and thus increases the temperature at the wick/core interface. Figure 16 also suggested that the liquid core is more vulnerable to vapor formation for the wick structure with a higher effective thermal conductivity. As shown in Figure 16, the temperature at the wick/core interface is much lower than the saturation temperature for an effective thermal conductivity of $1W/m \cdot K$ while it is greater than the saturation temperature for an effective thermal conductivity of $10W/m \cdot K$. Figure 17 shows the effect of effective thermal conductivity on the temperature at the core/bayonet interface. Increasing effective thermal conductivity increases the heat transfer to the core, and accordingly increases the heat dissipation from the core to the bayonet. As a result, the temperature in the bayonet increases with the effective thermal conductivity, as shown in Figure 17.

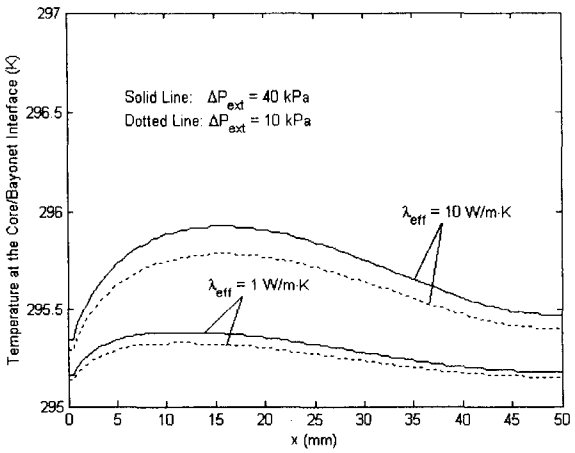

Figure 17- Influence of λ_{eff} and ΔP_{ext} on temperature at the core/bayonet interface ($q''_w = 30kW/m^2$, $\Delta T_{sub,li} = 5K$)

9. Conclusions

The loop heat pipe evaporators operating under steady state conditions were numerically investigated to describe evaporator characteristics and evaluate evaporator performance. Numerical solutions were obtained for conjugate flow and heat transfer in primary evaporator components. The numerical results indicated that in the liquid core the maximum temperature appears at the stagnation point of the wick/core interface, where the vapor may be generated on the inner wick surface. The subcooled liquid in the bayonet serves to be a heat sink for the liquid core, especially the liquid at the inlet of the bayonet which has the maximum subcooling level. Due to this cooling effect, the vapor present at the stagnation end of the liquid core can be collapsed by exchanging heat with the incoming subcooled liquid in the bayonet.

Two typical geometrical configurations used for the cylindrical LHP evaporator, non-bayonet evaporator and bayonet evaporator, were considered to examine the bayonet effects on evaporator operation. It was found that the presence of a bayonet forces any vapor present in the liquid core to flow to the inlet liquid end of the evaporator where it can be collapsed by exchanging heat with the incoming subcooled liquid in the bayonet. The presence of a bayonet significantly affects the flow and heat transfer in the liquid core and helps to prevent vapor bubbles from accumulating inside the core, which must be considered in the evaporator model.

Parameters affecting flow and heat transfer in the evaporator were studied. The influences of input heat flux, inlet liquid subcooling, external loop resistance and effective thermal conductivity of the wick structure were specifically selected to evaluate evaporator performance. It was observed that increasing the applied heat flux and inlet liquid subcooling decreases the maximum temperature in the liquid core and helps to prevent the vapor formation in the liquid core, which is favorable for proper evaporator operation. Decreasing the external loop resistance and the effective thermal conductivity of the wick structure also decreases the maximum temperature in the liquid core. Additionally, increasing the applied heat flux and liquid subcooling significantly enhances the cooling capability of the liquid in the bayonet. This helps prevent vapor bubbles from accumulating in the liquid core.

References

[1] Yu.F. Maidanik, State-of-the-art of CPL and LHP technology, in: Heat Pipe Science and Technology, Proceedings of 11th International Heat Pipe Conference, Tokyo, 1999, pp. 19-30.

[2] J.M. Ochterbeck, Heat pipes, in: A. Bejan and A. Kraus (Eds.), Handbook of Heat Transfer, John Wiley & Sons, New York, 2003, pp. 1181-1230.

[3] J. Ku, Operating characteristics of loop heat pipes, SAE Paper No. 1999-01-2007, July 1999.

[4] Y.H. Yan, J.M. Ochterbeck, Numerical investigation of the steady-state operation of a cylindrical capillary pumped loop evaporator, Journal of Electrical Packaging 125(3) (2003), 251-260.

[5] A.M. Kiper, G. Feric, M. Anjum, T.D. Swanson, Transient analysis of a capillary pumped loop heat pipe, AIAA Paper No. 90-1685, Proceedings of AIAA/ASME 5th Joint Thermophysics and Heat Transfer Conference, Seatle, WA, 1990.

[6] W.B. Bienert, D.A. Wolf, Temperature control with loop heat pipes: Analytical model and test results, Proceedings of the 9th International Heat Pipe Conference, Albuquerque, New Mexico, pp. 981-988, 1995.

[7] T. Kaya, T.T. Hoang, Mathematical modeling of loop heat pipes and experimental validation, Journal of Thermophysics and Heat Transfer 13(3) (1999), 314-320.

[8] H. Wultz, E. Embacher, Capillary pumped loops for space applications: Experimental and theoretical studies on the performance of capillary evaporator designs, AIAA Paper No. 90-1739, Proceedings of AIAA/ASME 5th Joint Thermophysics and Heat Transfer Conference, Seatle, WA, 1990.

[9] Y.D. Cao, A. Faghri, Analytical solutions of flow and heat transfer in a porous structure with partial heating and evaporation on the upper surface, International Journal of Heat and Mass Transfer 37(10) (1994) 1525-1533.

[10] Y.D. Cao, A. Faghri, Conjugate analytical of flat-plate type evaporator for capillary pumped loops with three-dimensional vapor flow in the groove, International Journal of Heat and Mass Transfer 37(3) (1994), 401-409.

[11] T.S. Zhao, Q. Liao, On capillary-driven flow and phase-change heat transfer in a porous structure heated by a finned surface: Measurements and modeling, International Journal of Heat and Mass Transfer 43(7) (2000) 1141-1155.

[12] D. Khrustalev, A. Faghri, Heat transfer in the inverted meniscus type evaporator at high heat fluxes, International Journal of Heat and Mass Transfer 38(16) (1995) 3091-3101.

[13] K.S. Udell, Heat transfer in porous media heated from above with evaporation, condensation, and capillary effects, Journal of Heat Transfer 105(2) (1983) 485-492.

[14] K.S. Udell, Heat transfer in porous media considering phase change and capillarity —

the heat pipe effect, International Journal of Heat and Mass Transfer 28(2) (1985), 485-495.

[15] A. Faghri, Heat Pipe Science and Technology, Taylor & Francis, Washington DC, 1995.

[16] Y.F. Maidanik, Y.G. Fershtater, Theoretical basis and classification of loop heat pipes and capillary pumped loops, Proceedings of the 10th International Heat Pipe Conference, Stuttgart, Germany, 1997.

[17] S.V. Patankar, Numerical Heat Transfer and Fluid Flow, McGraw-Hill, New York, 1980.